MINISTRY OF TECHNOLOGY

AERONAUTICAL RESEARCH COUNCIL
REPORTS AND MEMORANDA

The Effect of Change in Axial Velocity on the Potential Flow in Cascades

By M. R. A. Shaalan and J. H. Horlock

The Effect of Change in Axial Velocity on the Potential Flow in Cascades

By M. R. A. Shaalan and J. H. Horlock

Summary.

An analysis is given for the potential flow through a cascade in which a change in axial velocity occurs. An approximate solution of the derived potential equation is obtained and applied first to a flat plate cascade and then to a cascade of blades with camber and thickness. In the former application Weinig's exact solution is used as a first approximation while in the latter application Schlichting's analysis is used as a basic solution and then modified to account for the change in axial velocity.

Calculations demonstrate the effect of change in axial velocity on the cascade performance.

CONTENTS

1

1. Introduction.

Experimental cascade data is widely used in the design of axial flow compressors. Many attempts have been made to predict the performance of compressor cascades with varying degrees of success. Most potential-flow theories assume purely two-dimensional flow through the cascade, which is a reasonable assumption when the cascade is operating well away from stall. However experiments (Rhoden[1], Pollard[2], Shaalan[3]) have shown a remarkable flow contraction across the cascade when the side wall boundary layer is not removed. The increase in axial velocity, which is a measure of the contraction, may be some 30 to 40 per cent of the inlet axial velocity near the stalling point. This enormous contraction appears to be due to the boundary-layer separation initiated in the corner between the blade suction surface and the side wall of the wind tunnel. Such an acceleration severely limits the static-pressure rise that can be achieved by the cascade but it may at the same time delay stalling because of the reduction in the adverse pressure gradient through the centre of the cascade.

In order to predict the stalling incidence, the pressure distribution round the blade profile must be calculated as accurately as possible. In a two-dimensional flow, an inviscid-flow solution, with equal velocities on the upper and lower surfaces close to the trailing edge, is shown to be a good approximation to the real flow (Gostelow, Lewkowicz and Shaalan[4]). But for accurate determination of the pressure distribution, the effects of the three-dimensional contraction of the flow must be included.

Some attempts have been made to solve the potential flow including an axial velocity change. Montgomery[5] has created a reduction in axial velocity through a compressor cascade by placing an obstacle in the downstream flow and has also approached the problem theoretically, replacing the obstacle by a series of doublets. Bollard and Horlock[6]* have modified the two-dimensional analysis of Schlichting[7], including strip sources and sinks to account for the change in axial velocity. The strip singularities were of constant strength in both directions, normal to and along the cascade, producing a linear change in axial velocity within the cascade. Recently Norbury[8] has approached the problem by regarding each aerofoil as an element of an annular cascade. The radial flow, which corresponds to axial velocity in the conventional case, was obtained by locating an infinite line source or sink along the axis of the annulus. This he superimposed on a uniform axial flow and solved the problem for a single conical or near conical aerofoil. Two cases were considered, aerofoils of zero camber and thickness and aerofoils of zero thickness but with camber. Results for the circulation over a range of incidence and stagger are reported in Reference 8 for radially inward and outward flows.

In the present Report the problem is approached differently. The continuity equation is manipulated to arrive at a Poisson partial differential equation for the velocity potential. The solution of this equation follows that suggested by Price[9] for the case of compressible two-dimensional flow where a similar equation arises.

The method of solution is simplified and applied first to a flat-plate cascade then to a cascade of blades with camber and thickness. The latter application may be regarded as an improvement on Pollard and Horlock's modification of the Schlichting analysis.

2. Analysis.

2.1. The Equation for the Potential.

Figure 1 shows a diffusing flow through a cascade. An x, y, z co-ordinate system is used.
The continuity equation in three-dimensional incompressible flow is:

$$\frac{\partial C_x}{\partial x} + \frac{\partial C_y}{\partial y} + \frac{\partial C_z}{\partial z} = 0 \tag{1}$$

---

*Kubota, S., J.S.M.E. Bulletin, Vol. 5, No. 19 (1962), has also suggested that a change in axial velocity may be introduced by including sources whose strengths vary arbitrarily in the x-direction only. However, for a cascade of arbitrary aerofoils, he restricted the problem to the case of sources uniformly distributed in both the x and y directions.

where C_x is the axial velocity, C_y is the tangenital velocity and C_z is the spanwise velocity.
Since the flow is irrotational

$$\frac{\partial C_x}{\partial y} - \frac{\partial C_y}{\partial x} = 0,$$

and defining a potential function ϕ so that:

$$C_x = \frac{\partial \phi}{\partial x}, C_y = \frac{\partial \phi}{\partial y}, C_z = \frac{\partial \phi}{\partial z}$$

it follows that

$$\frac{\partial^2 \phi}{\partial x^2} + \frac{\partial^2 \phi}{\partial y^2} = -\frac{\partial C_z}{\partial z}. \tag{2}$$

The approximations made here involve the term on the right hand side of equation (2),

$$-\frac{\partial C_z}{\partial z} = -\frac{\partial^2 \phi}{\partial z^2}.$$

It is assumed that near the x-axis (the centreline of the cascade) the intersections of the stream surfaces with any (x,z) plane are lines passing through a common point 0 on the x-axis, which is taken as the origin.
It then follows approximately

$$\frac{C_z}{z} = \frac{C_x}{x} = \sqrt{\frac{C_x^2 + C_z^2}{x^2 + z^2}}$$

and

$$\frac{\partial C_z}{\partial z} = \frac{C_x}{x} + \frac{z}{x} \cdot \frac{\partial C_x}{\partial z}.$$

For points near the x-axis we may ignore the second term so that

$$\frac{\partial C_z}{\partial z} = \frac{C_x}{x}. \tag{3}$$

Hence, equation (2) may be written, for the flow close to the centreline

$$\frac{\partial^2 \phi}{\partial x^2} + \frac{\partial^2 \phi}{\partial y^2} = -\frac{1}{x} \left(\frac{\partial \phi}{\partial x} \right). \tag{4}$$

The equation may be solved as it stands if the location of the origin 0 is known. It may be assumed that the mean axial velocity across a blade pitch C_{x_m} obeys a simple 'source' relation near the axis $z = 0$

$$C_{x_m} x = \text{constant} = \frac{1}{K}. \tag{5}$$

Further if the axial velocity changes from $C_{x_{m1}}$ at the leading edge $(x = x_1)$ to $C_{x_{m2}}$ at the trailing edge $(x = x_2 = x_1 + a$, where a is the axial chord) and if the axial velocity ratio is $\lambda = C_{x_{m2}}/C_{x_{m1}}$, then

$$\frac{1}{K} = C_{x_{m1}} x_1 = C_{x_{m2}} x_2 = \lambda C_{x_{m1}} (x_1 + a). \qquad (6)$$

For $\lambda < 1$, $x_1 = \dfrac{\lambda a}{1-\lambda}$ and the location of the origin is determined for a diffusing axial velocity. A similar simple source analysis gives the location of 0 downstream of the cascade, for increasing axial velocity across the cascade.

There are several alternative forms of the potential equation (4), $V^2\phi = F(x,y)$. The function on the right hand side may be written

$$F = -\frac{1}{x} \frac{\partial\phi}{\partial x},$$

$$F = \frac{C_x}{C_{x_m}} \frac{dC_{x_m}}{dx} = \frac{d}{dx}(\log_e C_{x_m}) \frac{\partial\phi}{\partial x},$$

$$F = -KC_{x_m} \frac{\partial\phi}{\partial x} = -\left(\frac{1-\lambda}{\lambda a}\right) \frac{C_{x_m}}{C_{x_{m1}}} \frac{\partial\phi}{\partial x},$$

$$F = \frac{C_x}{h} \frac{dh}{dx} = \frac{d}{dx}(\log_e h) \frac{\partial\phi}{\partial x}. \qquad (7)$$

where h is the height of the mean streamline as it passes through the cascade.

It is probably a better approximation to assume that the product of axial velocity and channel width obeys the 'source' relation. In this case $C_{x_m}\left(\dfrac{d-2yt}{d}\right) x = \dfrac{1}{K}$, where d is the blade spacing and y_t half the thickness. The function F is then increased locally by a factor

$$\frac{d}{d-2y_t}$$

2.2. Solution of the Potential Equation.
Equation (4) may be written as

$$\frac{\partial^2\phi}{\partial x^2} + \frac{\partial^2\phi}{\partial x^2} = F(x,y).$$

Price[9] has given a method for solving numerically this type of Poisson equation, which also arises in two-dimensional compressible flow through cascades. A similar method of solution is followed here, but several simplifications are made.

The steps in the solution are as follows:

1. Solve $\dfrac{\partial^2\phi_0}{\partial x^2} + \dfrac{\partial^2\phi_0}{\partial y^2} = 0$ for ϕ_0, the incompressible two-dimensional solution, as a first approximation.

2. Evaluate the R.H.S. of (4), $F(x,y)$ from this first approximation.

3. Locate plane sources in the flow field, the strength of a source at any point x,y being equal to the R.H.S. of (6).

4. Obtain the induced velocities u_F, v_F at the profile boundaries (parallel and normal to the profile) due to these plane sources $F(x,y)$. (See Appendix A).

4

5. Locate a line of singularities at the profile to cancel the normal induced velocities.

6. Obtain the total induced velocities in the flow field due to the line singularities and to the plane sources.

7. Add the total perturbation velocities on to the basic flow and re-evaluate the R.H.S. of (4).

8. Iterate from 4 until convergence has been obtained.

9. Calculate the total induced velocities parallel to the profile at the blade surface and calculate the circulation.

10. Calculate the outflow angle and lift coefficient from this corrected circulation.

The application of this procedure to solve a compressible flow is very complicated. In particular, numerical calculation of the induced velocities u_F, v_F (Step 4 above) at the profile is difficult and because of this a simplification to the problem was sought. It is assumed in Step 4 (Appendix A) that the distribution of axial velocity (and hence the source strength) from the suction surface of one blade to the pressure surface of the next blade is linear with y at any x. This enables the area integral which gives the induced velocities to be evaluated analytically in the y direction before numerical integration in the x direction.

3. *Applications.*

Two applications of the analysis are given here, one to a cascade of flat plates and one to a cascade of cambered aerofoils with thickness. In the first application Weinig's exact solution to the incompressible flow through a cascade of flat plates[10] is developed to give the potential solution ϕ_0 required in the first approximation. In the second application, Schlichting's analysis[7] is used both for the basic incompressible flow and in the subsequent analysis.

3.1. *The Cascade of Flat Plates.*

The incompressible two-dimensional velocity distribution (C_{x_0}, C_{y_0}) obtained from Weinig's incompressible two-dimensional solution is given in Appendix B.

It is shown in Appendix A that the induced velocity on a plate or chord line, may be obtained approximately, equation (A3), if the source strength $(-K C_{x_m}(x) \dfrac{\partial \phi_0}{\partial x})$ on each of the two surfaces is known.

Using the two appendices the induced velocities associated with the first approximation, parallel and normal to the surface (x,y) may be obtained.

$$U_F(X,Y)/C_1 = \frac{-1}{2d} \sum_{x_1}^{x_2} \left[m \sin \beta \, I_1 + m \cos \beta \, I_2 \sinh \frac{2\pi}{d}(x-X) \right.$$

$$\left. + b \sin \beta \, I_3 + b \cos \beta \, I_4 \sinh \frac{2\pi}{d}(x-X) \right] \Delta x \tag{8}$$

and

$$V_F(X,Y)/C_1 = \frac{-1}{2d} \sum_{x_1}^{x_2} \left[m \cos \beta \, I_1 - m \sin \beta \, I_2 \sinh \frac{2\pi}{d}(x-X) \right.$$

$$\left. + b \cos \beta \, I_3 - b \sin \beta \, I_4 \sinh \frac{2\pi}{d}(x-X) \right] \Delta x \tag{9}$$

where $b = F_l(x) - F_u(x)$, the difference in source strength from suction to pressure surface,

$$m = F_u(x) - \frac{x}{d \tan \beta} \left[F_l(x) - F_u(x) \right]$$

and I_1, I_2, I_3 and I_4 are integrals given in Appendix A. The limits of integration x_1 and x_2 are taken as $0 \cdot 025\, l \cos \beta$ and $0 \cdot 990\, l \cos \beta$.

It is next required to distribute line vortices along the plate to cancel out the velocity v_F, so that the plate lies along a streamline in the flow.

After Schlichting[7] it is assumed that the distribution of vorticity along the chord is

$$\frac{\gamma(x')}{2C_1} = A_0 \cot \frac{\Theta}{2} + A_1 \sin \Theta + A_2 \sin 2\Theta + \ldots + A_{n-1} \sin(n-1)\Theta \qquad (10)$$

where A_0, A_1, A_2, ... A_{n-1} are Fourier coefficients to be determined, and $\Theta = \cos^{-1}(2x'/l - 1)$.

Using Schlichting's analysis and following his notation, it follows that the induced velocities due to $\gamma(x')$ are

$$\frac{U_\gamma}{C_1} = \sum_{i=0}^{i=n-1} A_i g_{\gamma_i}, \qquad (11a)$$

$$\frac{V_\gamma}{C_1} = \sum_{i=0}^{i=n-1} A_i f_{\gamma_i}^* \qquad (11b)$$

where g_{γ_i} and $f_{\gamma_i}^*$ are factors tabulated by Schlichting.

If the L.H.S. of equation (11b) is put equal to $-V_F/C_1$ from equation (9), then the coefficients A_1 may be obtained and the distribution of vorticity $\gamma(x')$ can be calculated.

The basic ϕ_0 flow, the flow due to the sources $-\frac{1}{x} \frac{\partial \phi_0}{\partial x}$ and the flow due to the vorticity $\gamma(x')$ may now be added together to give the resultant velocity on either plate surface.

$$C_s = C_{s_0} + u_F + u_\gamma \pm \gamma/2 \quad (+\text{ for suction side and } - \text{ for pressure side}) \qquad (12)$$

where C_{s_0} is the basic surface velocity.

(C_s may then be used for a second approximation. In the calculation described here, a second iteration has not been carried out because of the computation time involved).

With the vorticity distribution $\gamma(x')$ obtained, other cascade data follows. The change in tangenital velocity associated with the change in circulation $\int_0^l \gamma(x')\, dx'$ is

$$\Delta C_y = \pi \frac{l}{d} (A_0 + A_1/2)\, C_1 .$$

The modified inlet and outlet angles are then (see Fig. 2).

$$\tan \bar{\alpha}_1 = \frac{C_1 \sin \alpha_1 + \frac{1}{2} \Delta C_y}{C_1 \cos \alpha_1 / \left(\frac{\lambda+1}{2} \right)} = \frac{\lambda+1}{2} \left(\tan \alpha_1 + \frac{\frac{1}{2} \Delta C_y}{C_1 \cos \alpha_1} \right),$$

6

$$\tan \bar{\alpha}_2 = \frac{C_2 \sin \alpha_2 - \frac{1}{2} \Delta C_y}{C_{x_2}} = \frac{\lambda + 1}{2\lambda} \left(\tan \alpha_2 - \frac{\frac{1}{2} \Delta C_y}{C_1 \cos \alpha_1} \right)$$

where $\lambda = C_{x_2}/C_{x_1}$.
It may be shown that the lift coefficient is

$$C_L = 2 \, (d/l) \cos^2 \bar{\alpha}_1 \cos \beta \, (\tan \bar{\alpha}_1 - \lambda^2 \tan \bar{\alpha}_2) + (d/l) \cos^2 \bar{\alpha}_1 \sin \beta$$

$$\{(1 + \tan^2 \bar{\alpha}_1) - \lambda^2 \, (1 + \tan^2 \bar{\alpha}_2) + 2 \, (\lambda^2 - 1)\} \, .$$

The percentage change in circulation is

$$\Delta\Gamma \% = \left(\frac{\pi \, (l/d) \, (A_0 + A_1/2)}{\sin \bar{\alpha}_1 - \tan \alpha_2 \cos \alpha_1} \times \frac{\sin \bar{\alpha}_1}{(\sin \alpha_1 + (\frac{1}{2}) \, \Delta C_y/C_1)} \right) \times 100$$

and the modified pressure coefficient is

$$C_p = \frac{p - p_1}{\frac{1}{2} \rho \, \bar{C}_1^2} = 1 - \left(\frac{C_s}{\bar{C}_1} \right)^2 = 1 - \left[\frac{C_s}{C_1} \cdot \frac{C_1}{\bar{C}_1} \right]^2 \, .$$

It is worth noting that the pressure coefficient (and other quantities) obtained must be compared with that of two-dimensional flow with the inlet angle $\bar{\alpha}_1$, not α_1.

3.2. *The Cascade of Cambered Thick Aerofoils.*

The analysis for cambered aerofoils follows that of the flat plates, but Schlichting's analysis is used from the start for the two-dimensional flow. The aerofoil is replaced by a source-sink distribution $q_0(x')$ and a vorticity distribution $\gamma_0(x')$ along the chord line. The distributions are expressed as Fourier series and by matching the thickness slope and the camber-line slope at say n points, n Fourier coefficients in each series are determined.

The velocity distributions on the suction and pressure sides are:

$$C_{m_{x'}} + U_{q_0} + U_{\gamma_0} + \gamma_0/2 \, ,$$

$$C_{m_{x'}} + U_{q_0} + U_{\gamma_0} - \gamma_0/2$$

respectively
where U_{q_0}, U_{γ_0} are the induced velocities due to $q_0(x')$, $\gamma_0(x')$ respectively. The velocities on the profile surfaces are:

$$C_{s_{0u}} = \left(C_{m_{x'}} + U_{q_0} + U_{\gamma_0} + \gamma_0/2 \right) \Big/ \left(1 + \left(\frac{dy_u}{dx'} \right)^2 \right)^{\frac{1}{2}} ,$$

$$C_{s_{0l}} = \left(C_{m_{x'}} + U_{q_0} + U_{\gamma_0} - \gamma_0/2 \right) \Big/ \left(1 + \left(\frac{dy_l}{dx'} \right)^2 \right)^{\frac{1}{2}}$$

where y_u, y_1 are the ordinates of the suction and pressure surfaces.

From these velocities the plane source distribution $F(x,y)$ is calculated along both sides of the chord line and the induced components of velocity (u_F, v_F) due to $F(x,y)$ at the chord line are obtained as in application 3.1 and Appendix A.

Next additional line vortices $\gamma(x')$ and line sources and sinks $q(x')$ are located on the chord line to produce induced velocities u_γ, v_γ, u_q, v_q respectively.

7

These velocities are calculated using the Schlichting equations:

$$\frac{(u_q + u_\gamma)}{C_1} = \sum_{i=0}^{i=n=1} A_i\, g_{\gamma i} + B_0\, g_{q_0}^* + \sum_{i=2}^{i=n} B_i\, g_{q_i}^*,$$ (13a)

and

$$\frac{(v_q + v_\gamma)}{C_1} = \sum_{i=0}^{i=n=1} A_i f_{\gamma i}^* + B_0 f_{q_0} + \sum_{i=2}^{i=n} B_i f_{q_i}$$ (13b)

where B_1 are Fourier coefficients defined by the series:

$$\frac{q(x')}{2C_1} = B_0 \left(\text{Cot}\,\frac{\Theta}{2} - 2\sin\Theta\right) + \sum_{i=2}^{i=n} B_i \sin i\,\Theta$$ (14)

Θ and A_i are defined as in equation (10). Again g_i, g_q^r, f_1^r, f_q are factors tabulated by Schlichting. The slope of the camber line is now

$$\frac{dy_c}{dx'} = \frac{C_{m_{y'}} + (v_{q_0} + v_{\gamma_0}) + (v_q + v_\gamma) + v_F}{C_{m_{x'}} + (u_{q_0} + u_{\gamma_0}) + (u_q + u_\gamma) + u_F}.$$

and the slope of the thickness distribution is

$$\frac{dy_t}{dx'} = \frac{\tfrac{1}{2} q_0(x') + \tfrac{1}{2} q(x') - y_t \left(\dfrac{\partial u_F}{dx'} - F(x')\right)}{C_{m_{x'}} + (u_q + u_\gamma) + (u_{q_0} + u_{\gamma_0}) + u_F}.$$

These equations can be solved for n points to yield the unknown Fourier coefficients in the distributions $\gamma(x')$, $q(x')$. The corresponding velocities $(u_q + u_\gamma)$ and $(v_q + v_\gamma)$ are then obtained and the modified velocities on either side of the chord line are then known, and the velocity on the blade surface is obtained as in the normal two-dimensional solution.

The steps in calculating ΔC_y, $\Delta\Gamma$, $\bar\alpha_1$ and $\bar\alpha_2$ are all similar to those taken in solving the flat-plate problem.

4. *Calculations.*

4.1. *The Flat-Plate Cascade.*

Fig. 3 shows the pressure distribution obtained from Weinig's solution for a flat-plate cascade of space-chord ratio 0·875, set at a stagger of 36° and an incidence of 20° for which $\alpha_2 = 36\cdot75°$.

Fig. 4 shows the distributions of induced velocities due to plane sources calculated from the first approximation and Fig. 5 shows the perturbation vorticity distribution along the chord. The percentage change in circulation is $\Delta\Gamma\% = -7\cdot50$. Fig. 6 shows the distribution of chordwise components of velocity due to line vortices on chord.

It follows that

$$\bar\alpha_1 = 57\cdot30°, \bar\alpha_2 = 36\cdot30°.$$

Fig. 7 shows a comparison between the pressure distributions when there is an increase in axial velocity of 15 per cent of a decrease of 20 per cent for the same inlet angle.

4.2. *The Cambered Aerofoil with Thickness.*

The flow past a cascade of aerofoils of profile 10C430C50, set at a stagger β of 36° and a space-chord ratio of 0·875, was calculated. The inlet angle α_1 was assumed to be 52·00 in the preliminary two-dimensional Schlichting calculation.

Fig. 8 shows the distribution of induced velocities at the chord line due to plane sources $F(x,y)$ calculated from the first approximation.

The modified pressure distribution C_p is shown in Fig. 9 for $\lambda = 1·10$ and $\lambda = 0·90$. The corresponding air angles are

$$\bar{\alpha}_1 = 52·80°, \bar{\alpha}_2 = 28·50° \,(\lambda = 1·10).$$

For a two-dimensional flow with the same inlet angle $\alpha_1 = \bar{\alpha}_1 = 52·80°$, the outlet angle $\alpha_2 = 29°$ and the pressure distribution is as shown in Fig. 9.

5. *Conclusions.*

A method is given for calculating the pressure distribution and fluid deflection in a cascade across with a change in axial velocity takes place. It is shown that there are substantial changes in these quantities with axial velocity ratio ($\lambda = C_{x_2}/C_{x_1}$). In particular the diffusion on the suction surface of the blade is altered considerably.

It is particularly important to realise that the value of λ increases towards the stall point because of end wall effects in the cascade, and any two-dimensional calculations of boundary-layer development and separation are not valid unless the effects of axial velocity ratio are included.

The method described is approximate in two ways

(a) a linear distribution of equivalent source strength from blade to blade is assumed.

(b) an approximate result is used for one of the integrals in the analysis. However it is submitted that the analysis is sufficiently accurate for practical purposes.

A comparison is given in Fig. 10 between calculations based on the present analysis and the analysis of Ref. 6. The difference between the two pressure distributions occurs mainly on the front part of the suction side due to the inclusion of a non-uniform source distribution in the flow field.

It should be noted that a simple extension of the analysis enables a solution to the compressible flow in cascades to be obtained (an approximate solution of the problem as posed by Price[9]). Details of this work form the subject of another paper.

6. *Acknowledgements.*

LIST OF SYMBOLS

Analysis.

x,y,z	Reference axes (axial, tangenital and spanwise directions respectively)
C_x, C_y, C_z	Velocity components in the directions of the reference axes
r	Radial distance in the source flow
θ	Angle included between the x-axis and the source streamline
λ	Axial velocity ratio $\left(\dfrac{\text{outlet axial velocity}}{\text{inlet axial velocity}} \right)$
h	Height of mean streamline
a	Axial chord length
F	Plane source strength
ϕ	Potential function
K	Constant defined in text

Applications and Appendices.

x', y'	Cartesian Co-ordinates with the actual chord as x'-axis and leading edge as origin
u, v	Velocity components in the directions x', y'
(X, Y)	A point at the plate
d/l	Space chord ratio
y_t	Blade thickness
y_c	Blade camber
y_u	Upper surface co-ordinate
y_l	Lower surface co-ordinate
ϕ_0	Basic velocity potential
C_{x_0}, C_{y_0}	Basic velocity components at plate
C_1	Inflow velocity
C_2	Outflow velocity
$\bar{C}_1$	Inflow modified velocity (2nd approximation)
$C_{s_{0u}}$	Velocity on the upper surface
$C_{s_{0l}}$	Velocity on the lower surface
$C_{m_{x'}}$	Basic mean flow velocity in the direction of x'
$C_{m_{y'}}$	Basic mean flow velocity in the direction of y'
$\left.\begin{array}{c} u_{\gamma_0}, v_{\gamma_0} \\ u_{q_0}, v_{q_0} \end{array}\right\}$	Induced velocity components at chord due to basic singularities
$\left.\begin{array}{c} u_\gamma, v_\gamma \\ u'_q, v_q \end{array}\right\}$	Induced velocity components at chord due to perturbation singularities

u_F, v_F	Induced velocity components at chord due to plane sources
C_{x_1}	Inlet axial velocity
C_{x_2}	Outlet axial velocity
C_s	Resultant modified velocity at plate
C_{s_0}	Basic flow velocity at plate
ΔC_y	Increment change in the tangenital velocity due to perturbation singularities
α_1	Inlet flow angle (1st approximation)
α_2	Outlet flow angle (1st approximation)
$\bar{\alpha}_1$	Modified outlet flow angle
$\bar{\alpha}_2$	Modified outlet flow angle
Θ	Profile parameter (defined by Equation 10)
S, C	Hyperbolic functions defined in Appendix A
s, c	Trigonometric functions defined by Appendix A
β	Stagger angle
C_L	Lift coefficient $= \dfrac{L \text{ (lift force)}}{\frac{1}{2}\rho \bar{C}_1^2 . l}$.
Γ	Circulation
$\Delta\Gamma$	Increment change in circulation
p	Surface local static pressure
p_1	Inlet static pressure
ρ	Fluid density
C_p	Static-pressure coefficient $= (p/p_1)/\frac{1}{2}\rho \bar{C}_1^2$.
$\gamma_0(x'), q_0(x)$	Basic singularity distribution in Schlichting's analysis
$\gamma(x'), q(x')$	Perturbation singularities to account for the change in axial velocity
n	Number of stations on chord to define the profile
b, m	Constants used in the approximation
ε	Angle defined in Appendix A
I_1, I_2, I_3, I_4	Integrals associated with the approximation
A_i, B_i	Fourier coefficients
$\left.\begin{array}{l} g_{\gamma i}, f_{\gamma i}^* \\ g_{q i}^*, f_{q i} \end{array}\right\}$	Factors defined in Schlichting's analysis

Subscripts.

1	Inlet condition (or L.E. condition)
2	Outlet condition (or T.E. condition)
s	Refers to surface

11

u	Refers to upper surface (suction)	
l	Refers to lower surface (pressure)	
F	Associated with plane source distribution	
o	Basic value	
γ	Associated with vorticity distribution	
q	Associated with line source distribution	
n	Associated with n^{th} coefficients	
i	Associated with i^{th} coefficient	

REFERENCES

No.	Author(s)	Title, etc.
1	H. G. Rhoden	Effects of Reynolds number on the flow of air through a cascade of compressor blades. A.R.C. R. & M. 2919, July 1952.
2	D. Pollard	Low speed performance of two-dimensional cascades of aerofoils. Ph.D. Thesis, University of Liverpool. 1964.
3	M. R. A. Shaalan	The stalling performance of cascades of different aspect ratios (unpublished). 1966.
4	J. P. Gostelow, A. K. Lewkowicz and M. R. A. Shaalan	Viscosity effects on the two-dimensional flow in cascades. A.R.C., C.P. 872. October 1965.
5	S. R. Montgomery	Spanwise variations of lift in compressor cascades. Jl. Mech. Eng. Sci. Vol. 1. 1959.
6	D. Pollard and J. H. Horlock	A theoretical investigation of the effect of changes in axial velocity on the potential flow through a cascade of aerofoils. A.R.C., C.P. 619. June 1962.
7	H. Schlichting	Berechnug der reibungslosen inkompressiblen stromug fur ein vorgegevenes ebenes schaufelgitter. V.D.I. Forschungshaft 447. 1955.
8	J. F. Norbury	The circulation about a thin annular aerofoil in an axial stream with axial source or sink. ULME/B.4. February 1964.
9	D. Price	Two dimensional compressible potential flow around profiles in cascade. G.T.C.C. Aero. Sub. Committee Rep. 547.
10	F. Weinig	Die stromung um die schaufeln von turbomachinen. Joh. Ambr. Barth. Leipzig. 1935.

The Induced Velocity on the Chord Line due to the Distributed Sources.

Fig. 11 shows the induced velocities u_F and v_F parallel and normal to the chord line of the blades due to distributed sources of strength $F(x,y)$. Price[9] has shown that the induced velocity on the surface at (X,Y) due to source patterns repeating to infinity is

$$u_F(X,Y) = -\int_0^d \int_{-\infty}^{+\infty} \frac{F(x,y)\left(\sin\beta\sin\frac{2\pi}{d}(y-Y)+\cos\beta\sinh\frac{2\pi}{d}(x-X)\right)}{2d\left(\cosh\frac{2\pi}{d}(x-X)-\cos\frac{2\pi}{d}(y-Y)\right)}\,dx\,dy$$

(A1)

$$v_F(X,Y) = -\int_0^d \int_{-\infty}^{+\infty} \frac{F(x,y)\left(\cos\beta\sin\frac{2\pi}{d}(y-Y)-\sin\beta\sinh\frac{2\pi}{d}(x-X)\right)}{2d\left(\cosh\frac{2\pi}{d}(x-X)-\cos\frac{2\pi}{d}(y-Y)\right)}\,dx\,dy.$$

It is next assumed that $F(x,y)$ varies linearly from $F_u(x)$ on the suction surface to $F_l(x)$ on the pressure surface at a given x

i.e. $F(x,y) = \left(\dfrac{F_l(x)-F_u(x)}{d}\right)\cdot y + \left[F_u(x)-\dfrac{y_u}{d}(F_l(x)-F_u(x))\right]$

so by substitutions

$$u_F(X,Y) = -\int_{x_1}^{x_2}\int_{y_u}^{y_u+d}\frac{m+b(f)}{2d}\cdot\frac{\sin\beta\cdot s+\cos\beta\cdot S}{C-c}\,dy\,dx,$$

(A2)

$$v_F(X,Y) = -\int_{x_1}^{x_2}\int_{y_u}^{y_u+d}\frac{m+b(f)}{2d}\cdot\frac{\cos\beta\cdot s-\sin\beta\cdot S}{C-c}\,dy\,dx$$

where

$$s = \sin\frac{2\pi}{d}(y-Y),\quad S = \sinh\frac{2\pi}{d}(x-X),$$

$$c = \cos\frac{2\pi}{d}(y-Y),\quad C = \cosh\frac{2\pi}{d}(x-X),$$

$$m = F_u(x)-\frac{y_u}{d}\left(F_l(x)-F_u(x)\right),\quad b = F_1(x)-F_u(x),$$

$$y_u = \frac{t}{\tan\beta},\ f=\frac{y}{d}$$

The integration with respect to y may be obtained analytically, and the subsequent integration with respect to x is carried out numerically.

Equation (A2) can be written:

$$u_F(X,Y) = -\frac{1}{2d} \sum_{x_1}^{x_2} (m \sin \beta\, I_1 + m \cos \beta\, S\, I_2 + b \sin \beta\, I_3 + b \cos \beta\, S\, I_4)\, \Delta x ,$$

(A3)

$$v_F(X,Y) = -\frac{1}{2d} \sum_{x_1}^{x_2} (m \cos \beta\, I_1 - m \sin \beta\, S\, I_2 + b \cos \beta\, I_3 - b \sin \beta\, S\, I_4)\, \Delta x$$

where

$$I_1 = \int_{y_u}^{y_u+d} \frac{\sin \frac{2\pi}{d}(y-Y)}{C - \cos \frac{2\pi}{d}(y-Y)}\, dy ,$$

$$I_2 = \int_{y_u}^{y_u+d} \frac{1}{C - \cos \frac{2\pi}{d}(y-Y)}\, dy ,$$

$$I_3 = \int_{y_u}^{y_u+d} \frac{(y/d) \sin \frac{2\pi}{d}(y-Y)}{C - \cos \frac{2\pi}{d}(y-Y)}\, dy ,$$

$$I_4 = \int_{y_u}^{y_u+d} \frac{(y/d)}{C - \cos \frac{2\pi}{d}(y-Y)}\, dy .$$

(A4)

It may be shown that these integrals are

$$I_1 = 0 ,\ I_2 = \frac{d}{\sqrt{C^2-1}} ,\ I_3 = \frac{d}{2\pi} ln \left(\frac{C - \cos \varepsilon}{f(C)} \right) ,$$

$$I_4 = \frac{d}{\sqrt{C^2-1}} \left[\frac{1}{2\pi} \tan^{-1} \left(-\frac{\sqrt{C^2-1} \sin \varepsilon}{1 - C \cos \varepsilon} \right) + \frac{y_u}{d} \right]$$

(A5)

where

$$f(C) \simeq C^{\frac{1}{2}} . (C-1)^{\frac{1}{4}} . (C+1)^{\frac{1}{4}} ,$$

$$\varepsilon = \frac{2\pi}{d}(y_u - Y) ,$$

I_1, I_2 and I_4 are exact. No analytical solution for I_3 has been obtained, but the approximate result given is obtained by graphical plotting and use of the other integrals.

14

APPENDIX B

Weinig's Two-Dimensional Solution for the Flat Plate Cascade.

Weinig[10] gave an early exact solution for the flow past a cascade of flat plates. He used the method of conformal transformation, from the cascade plane to the region outside a circle.

Using the notation of Fig. 12 it may be shown by developing Weinig's analysis that the velocities C_{x_0}, C_{y_0} at the point (x,y) are given by:

$$\frac{C_{x_0}}{C_m} = \frac{1}{C_m}\frac{\partial \phi_0}{\partial y} = [w_0 \cos \delta + (w_1 + w_2)\sin \delta] \times \left.\left|\frac{d\zeta}{dz}\right|\right|_{(x,y)} \times \cos \beta, \tag{B1}$$

$$\frac{C_{y_0}}{C_m} = \frac{1}{C_m}\frac{\partial \phi_0}{\partial y} = [w_0 \cos \delta + (w_1 + w_2)\sin \delta] \times \left.\left|\frac{d\zeta}{dz}\right|\right|_{(x,y)} \times \sin \beta \tag{B2}$$

where

$$w_0 = \frac{4R}{[(R^2+1)^2 - 4R^2\cos^2\theta]}\left[(R^2-1)\sin\beta\cos\theta - (R^2+1)\cos\beta\sin\theta\right] \times \frac{d}{2\pi},$$

$$w_1 = \frac{-4R}{[(R^2+1)^2 - 4R^2\cos^2\theta]}\left[(R^2+1)\sin\theta\sin\beta + (R^2-1)\cos\theta\cos\beta\right] \times \frac{d}{2\pi},$$

$$w_2 = \frac{4R}{[(R^2+1)^2 - 4R^2\cos^2\theta]}\left[(R^2+1)\sin\theta_{st}\sin\beta + (R^2-1)\cos\theta_{st}\cos\beta\right] \times \frac{d}{2\pi},$$

$$\theta_{st} = \tan^{-1}\left[\tan\beta\left(\frac{R^2-1}{R^2+1}\right)\right],$$

$$\left|\frac{d\zeta}{dz}\right| = \frac{\pi}{d}\sqrt{\frac{X_2^2 + Y_2^2}{X_1^2 + Y_1^2}}$$

where

$$X_1 = R\cos 2\theta - \frac{1}{R}\left[1 + \cos 2\beta(R^2 - \cos 2\theta) + \sin 2\beta \sin 2\theta\right],$$

$$Y_1 = R\sin 2\theta - \frac{1}{R}\left[R^2 - \cos 2\theta \sin 2\beta - \cos 2\beta \sin 2\theta\right],$$

$$X_2 = (R^2 + \frac{1}{R^2})\cos 2\theta - 1 + \sin^2 2\theta - \cos^2 2\theta \text{ and}$$

$$Y_2 = (R^2 + \frac{1}{R^2} - 2\cos 2\theta)\sin 2\theta.$$

θ is varied from θ_{st} to $\theta_{st} + 2\pi$ to obtain the suction and pressure sides successively.
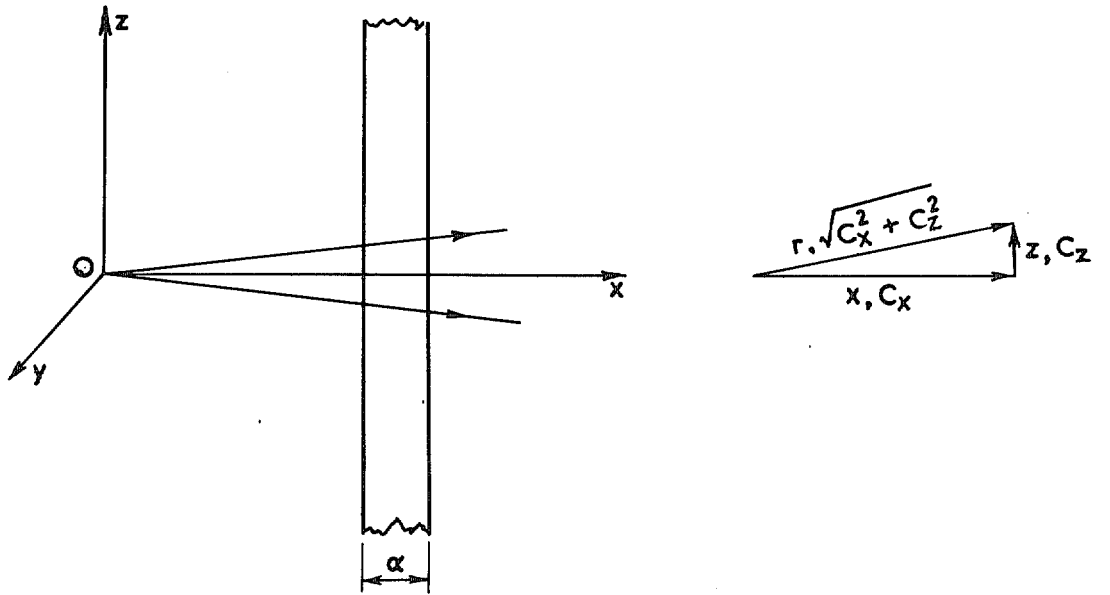
FIG. 1.   Diffusing flow model ($\lambda < 1$).
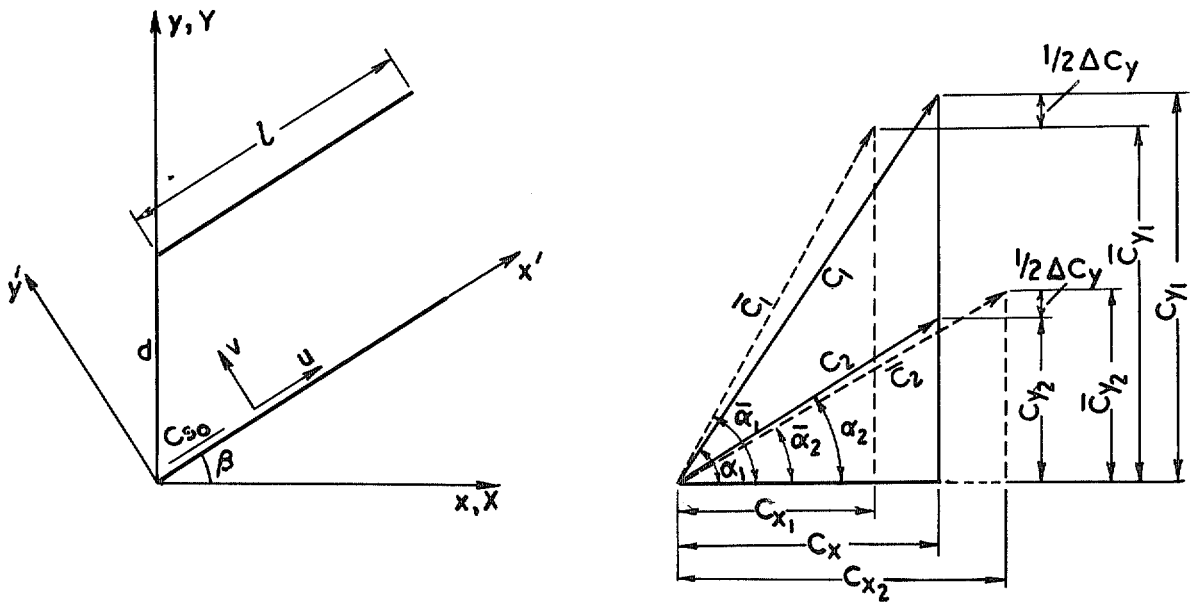
FIG. 2.   Co-ordinates and velocity diagrams.

16
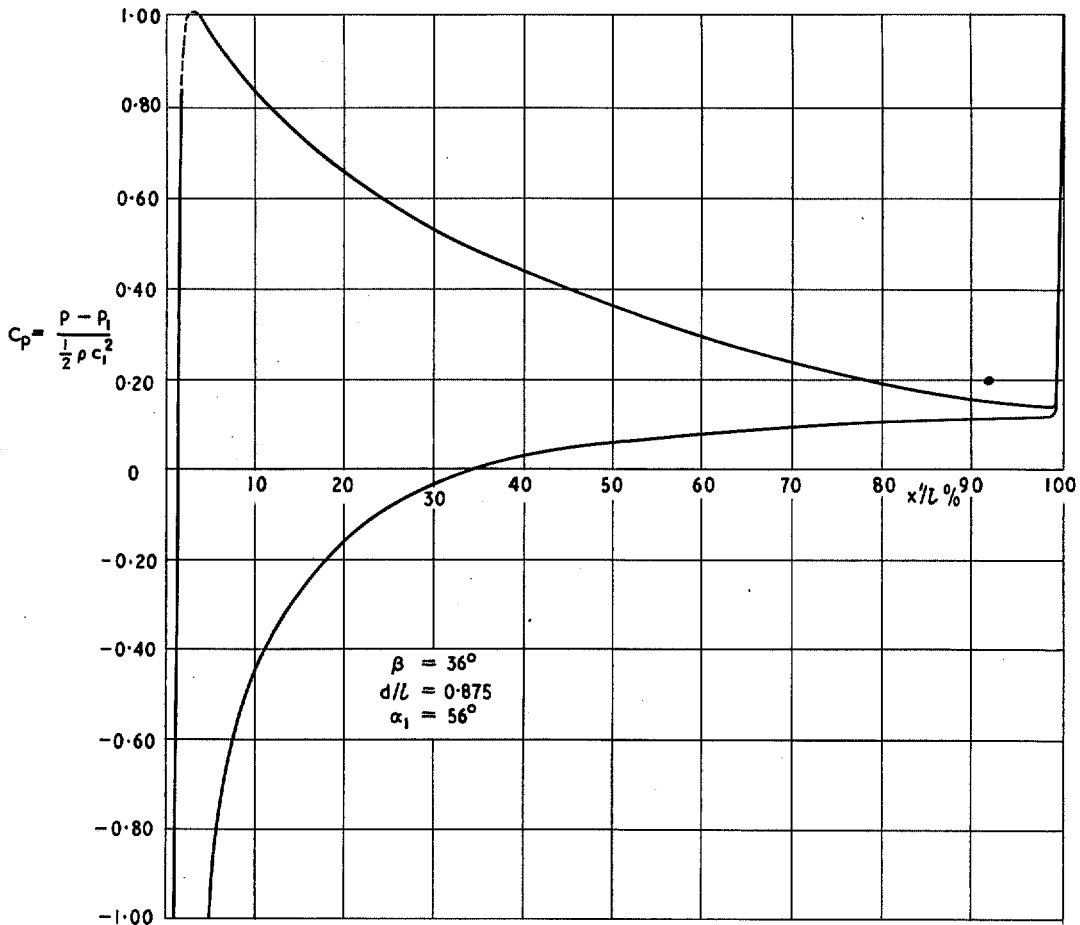
FIG. 3.   Pressure distribution (Weinig's solution).
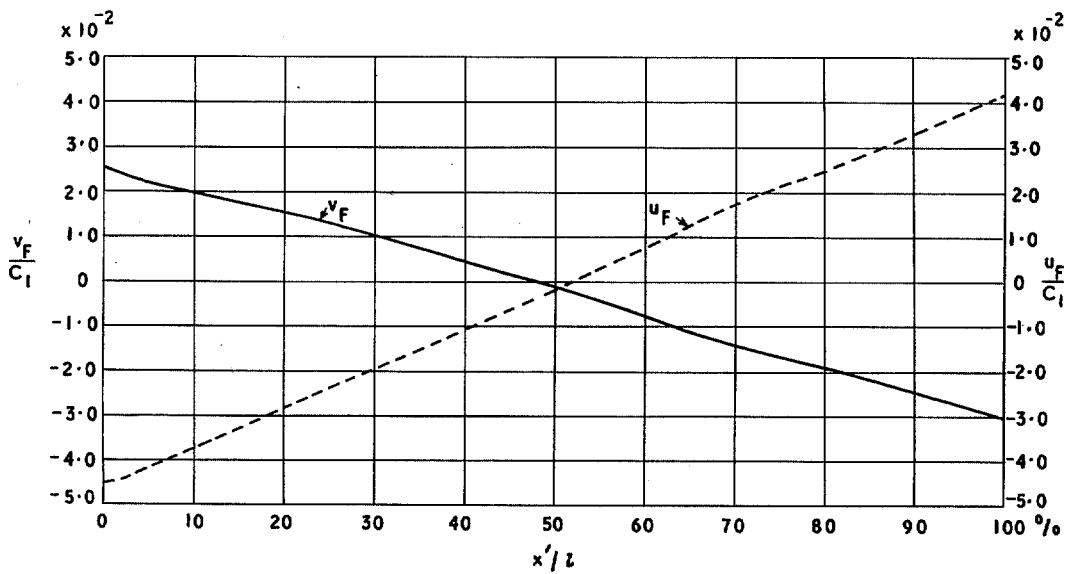
FIG. 4.   Normal and chordwise components of velocity induced at the flat plate due to plane sources
$(\alpha_1 = 56°, \lambda = 1\cdot15)$.

17
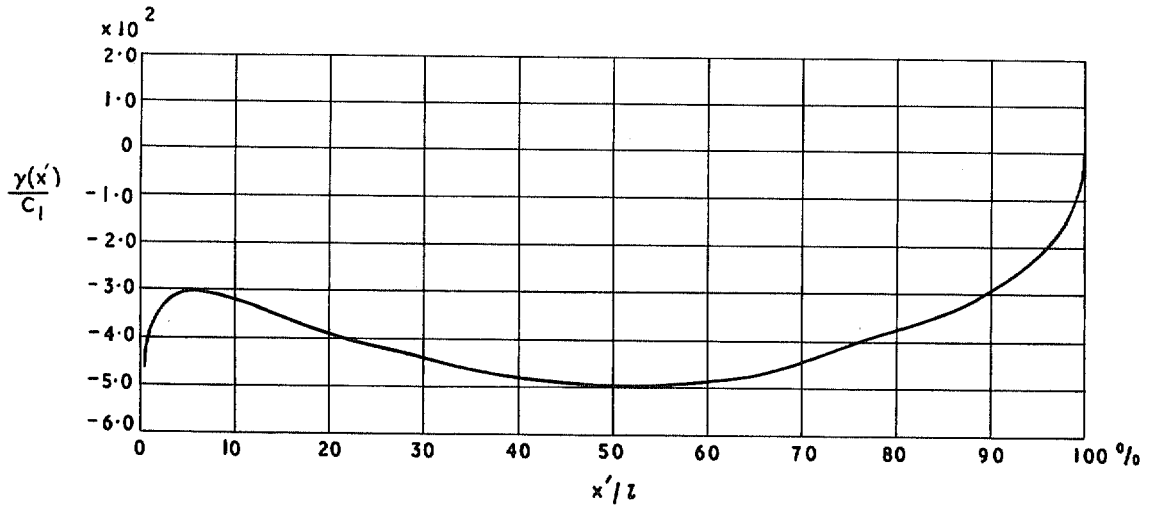
FIG. 5.   Perturbation vorticity distribution along the chord for flat plate cascade ($\alpha_1 = 56°$, $\lambda = 1·15$).
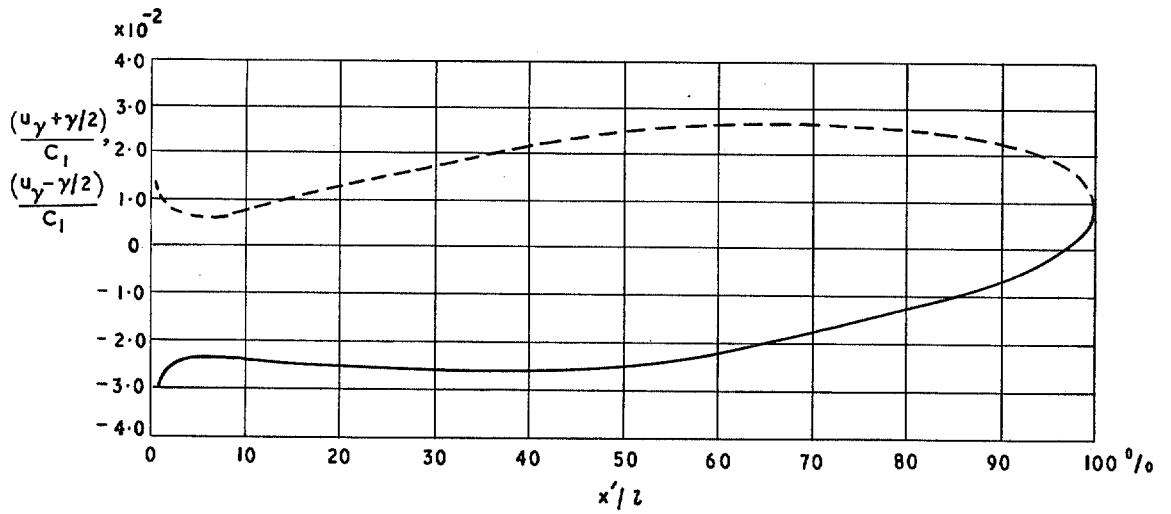
FIG. 6.   Induced velocities at the plate due to perturbation vorticity ($\alpha_1 = 56°$, $\lambda = 1·15$).

18
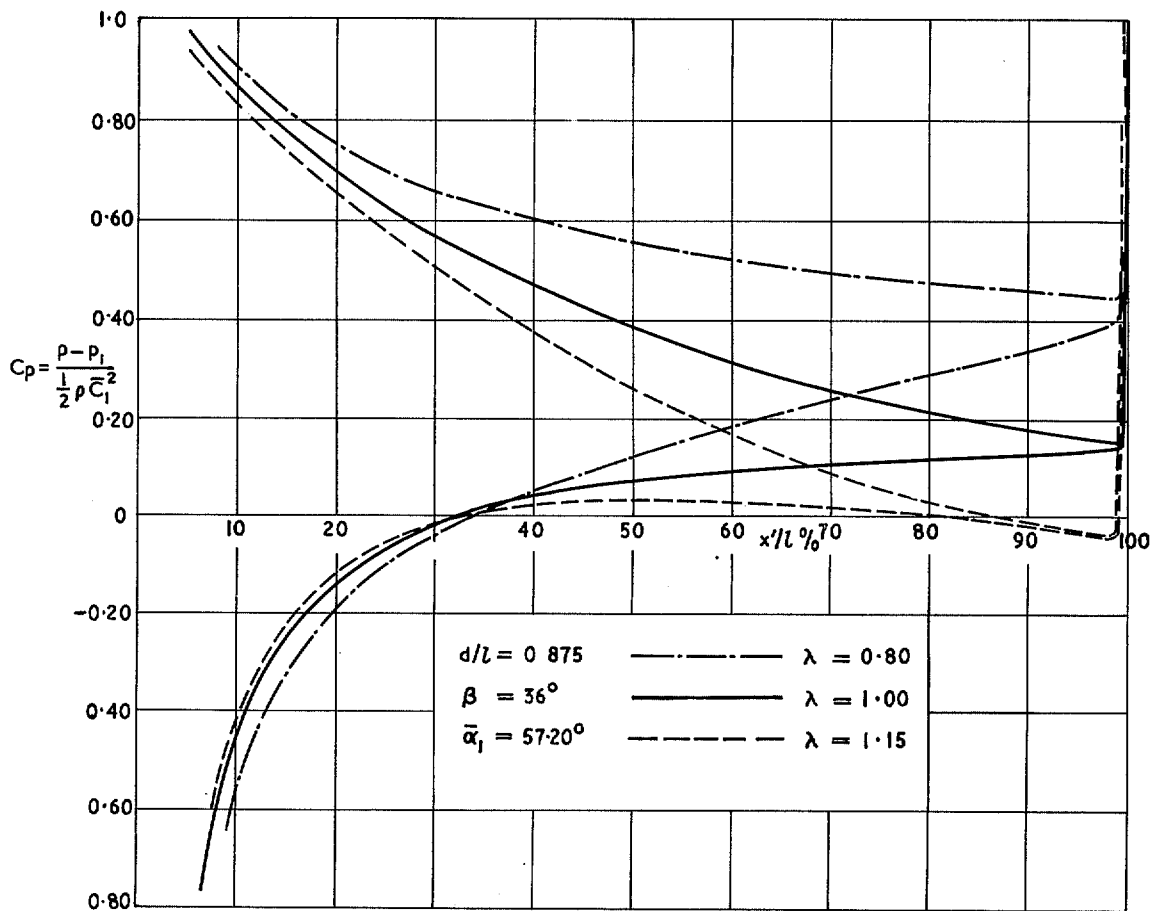
FIG. 7.   Effect of axial velocity change on pressure distribution (flat plate).
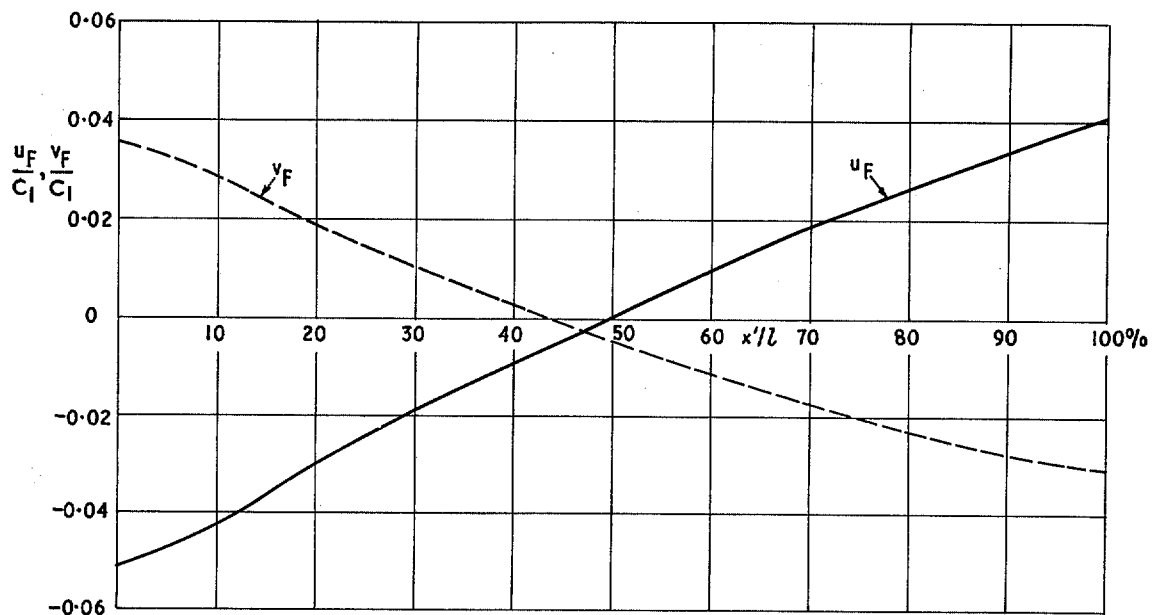
FIG. 8.   Induced velocities on chord due to plane sources. (10C4–30C50 blade).
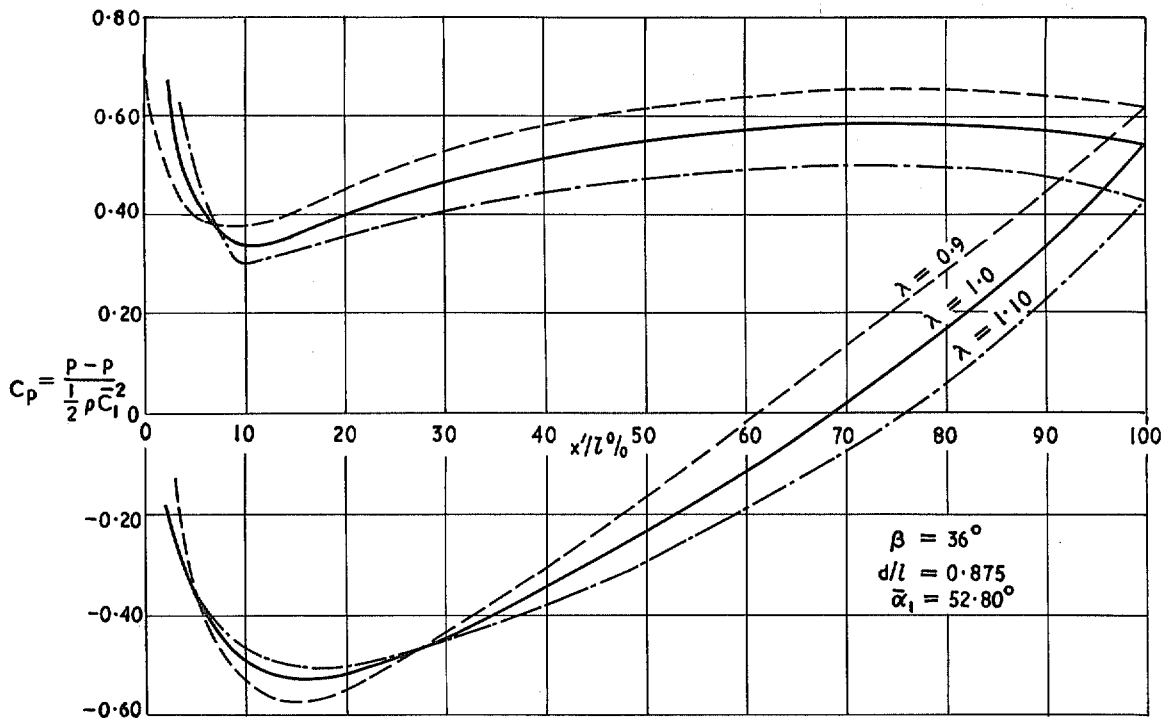
FIG. 9. Effect of axial velocity change on pressure distribution. (Cambered aerofoil with thickness).
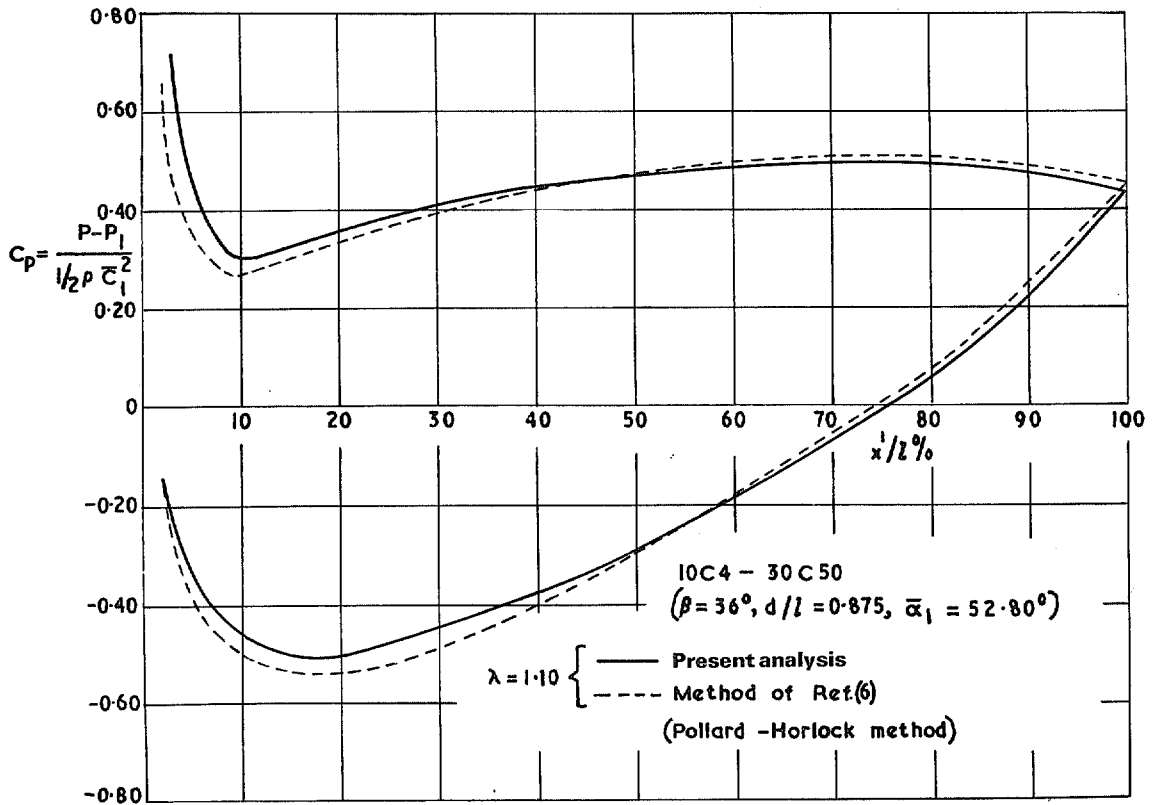
FIG. 10. Pressure distribution. Comparison between the present analysis and that of Ref. 6.

20
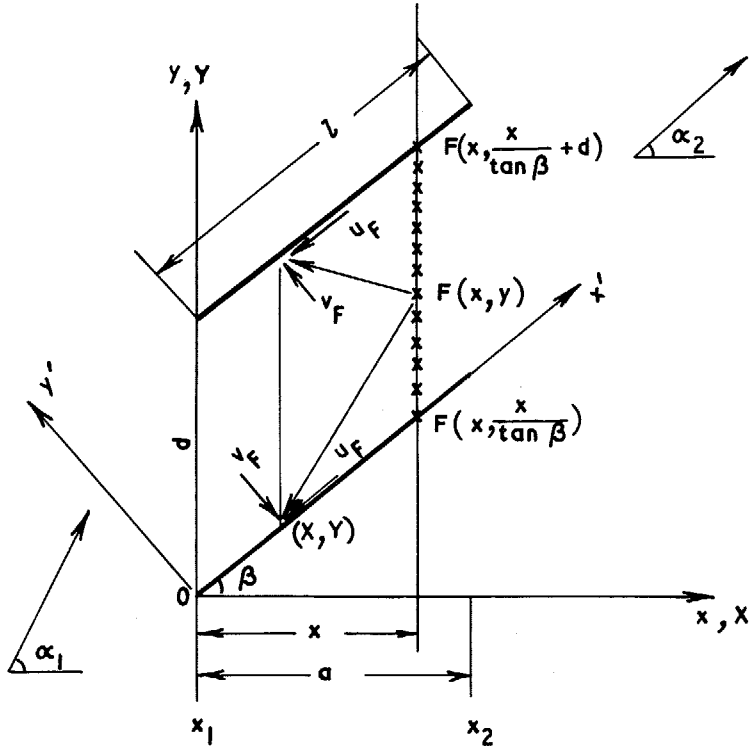
FIG. 11.   Velocities on plate (or chord) induced by plane sources.
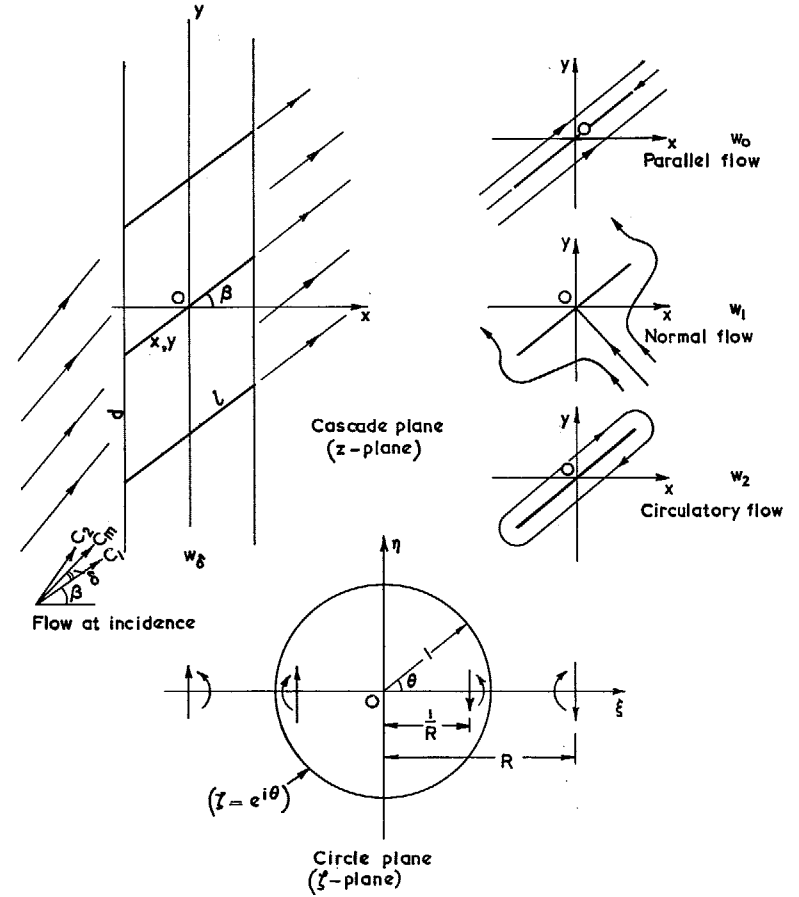
FIG. 12.   Conformal transformation of the flat plate cascade as given by Weinig (Ref. 10).